



STRUCTURAL
BIOLOGY

Volume 78 (2022)

Supporting information for article:

Structural visualization of transient interactions between the *cis*-acting acyltransferase and acyl carrier protein of the salinomycin modular polyketide synthase

Y. Feng, F. Zhang, S. Huang, Z. Deng, L. Bai and J. Zheng

Table S1 Primer list

Primers	Sequence (5'→3')
<i>SalAT9F</i>	atcgtaatccatattggacgcccccccctcgcggaggtgctcgeccc
<i>SalAT9R</i>	tgattc gatgaattcactggaaggcgtaggtcggcaggtcgaccacc
<i>SalAT9S190C-F</i>	cggacgcggtggtcggctcactgccagggtgagatcgcggct
<i>SalAT9 S190C-R</i>	gtgaccgaccaccgcgtccggcaccacaccggcggcgc
<i>SalAT9Q105A-F</i>	cggtgttcgtctcccggtgcgggtcgcagtgggccgg
<i>SalAT9Q105A-R</i>	accggggaagacgaacaccgtcttccggagaggtccg
<i>SalAT9R286A-F</i>	agttggaggccgaggggtgctcggcgaaggatcggctc
<i>SalAT9R286A-R</i>	gacaccctcggcctccaactcggccaccagctctcca
<i>SalAT9C298S-F</i>	gctcaggtggaccgcctgcacgagcggatcctcgacct
<i>SalAT9C298S-R</i>	tgcagcgggtccacctgagcgtgtgcgagggcaccgtgga
<i>SalAT9C347S-F</i>	cttcgtactggttcgagaacagccgcccccggctcagcttc
<i>SalAT9C347S-R</i>	gttctcgaaccagtacgaagcgtccaactcggcggcgt
<i>SalAT9Y379A-F</i>	gtcgcacccgggtgctgaccgc cggcatcagcgagaccgc
<i>SalAT9Y379A-R</i>	ggtcagcaccgggtgcgactcgaactccacgaacacgt
<i>SalAT9R399A-F</i>	tcctcgcgcagggcaccctggc gcgcgaggagggcgggct
<i>SalAT9R399A-R</i>	caggggtccctgcgcgaggacctcccggcccggcct
<i>SalAT9R399E-F</i>	tcctcgcgcagggcaccctggagcgcgaggagggcgggct
<i>SalAT9R399E-R</i>	caggggtccctgcgcgaggacctcccggcccggcct
<i>SalAT9R400A-F</i>	tcgcgcagggcaccctcggggccgaggagggcgggctcgc
<i>SalAT9R400A-R</i>	ccgcaggggtccctgcgcgaggacctcccggcccggc
<i>SalACP9F</i>	gcagatatacatatgggcgcgcgacccccggc
<i>SalACP9R</i>	gtggtggaattcacaggacggcggccccgag
<i>SalACP9D46T-F</i>	cctcaagaacctgggttcacctcgtcaccgcggctc
<i>SalACP9D46T-R</i>	gaagcccaggttcttgaagcccccccgggttcgatgt
<i>SalACP9E52A-F</i>	cgactcgtcaccgcggctcgcgctcgggaccgcctcgg
<i>SalACP9E52A-R</i>	cgaccgcgggtgagcagtcgaagcccaggttcttgaag
<i>SalACP9E52R-F</i>	cgactcgtcaccgcggctcgtcgtcgggaccgcctcgg

*Sal*ACP9E52R-R cgaccggtgagcgagtcgaagcccaggttctgaag

*Sal*ACP9R54A-F cgctcaccggtcgagctggcggaccgcctcggcgccgc

*Sal*ACP9R54A-R cagctcaccggtgagcgagtcgaagcccaggttct

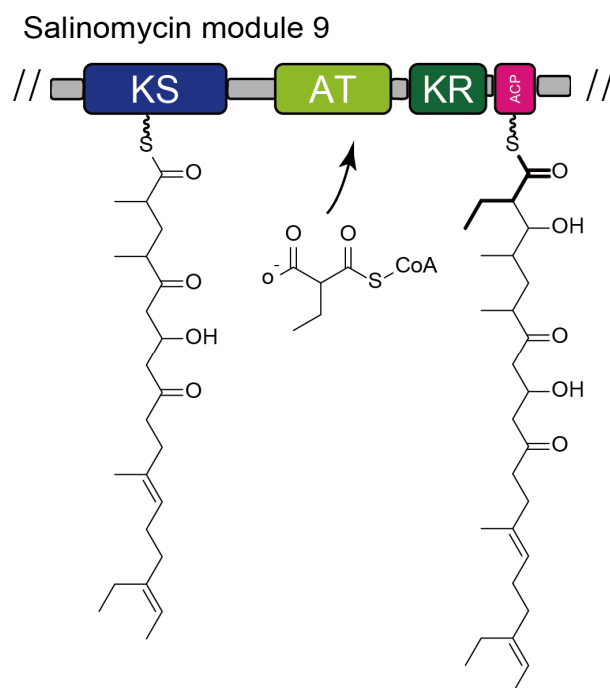


Figure S1 Domain organization of the 9th module of salinomycin mPKS. The module contains a *cis*-AT domain that selects ethylmalonyl-CoA extender unit.

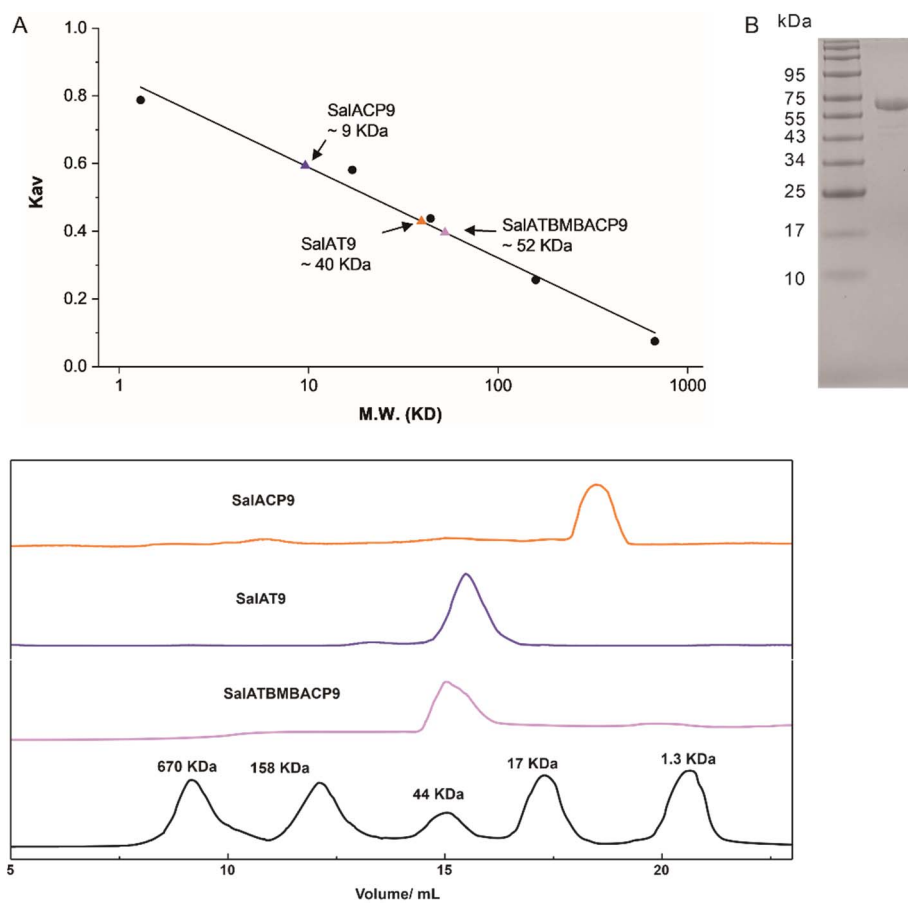


Figure S2 Molecular weights of purified proteins estimate by size-exclusion chromatography. (A) SalAT9M migrates at ~40 kDa (expected monomer mass: 48 kDa); SalACP9 migrates at ~9 kDa (expected monomer mass: 12 kDa); and SalAT9M-ACP9 migrates at ~52 kDa (expected monomer mass: 60 kDa). (B) SDS-PAGE of the purified SalAT9M-ACP9 complex.

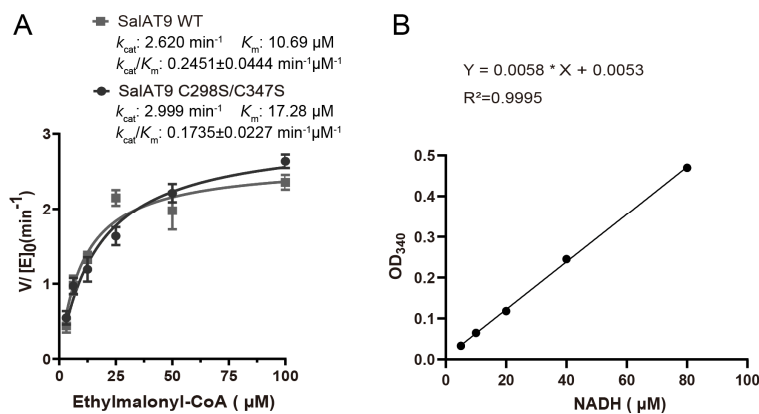


Figure S3 Kinetic analysis of SalAT9 and its mutant. (A) SalAT9 and its C298S/C347S mutant show similar kinetic parameters. (B) The standard curve for NADH. This curve was used for the calculate the rates of the AT-catalysed reactions.

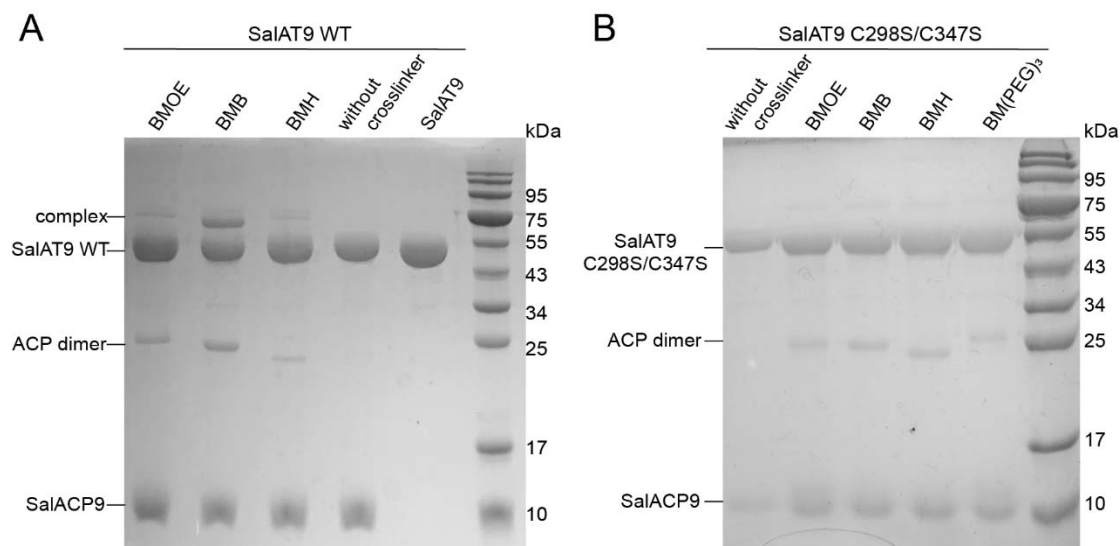
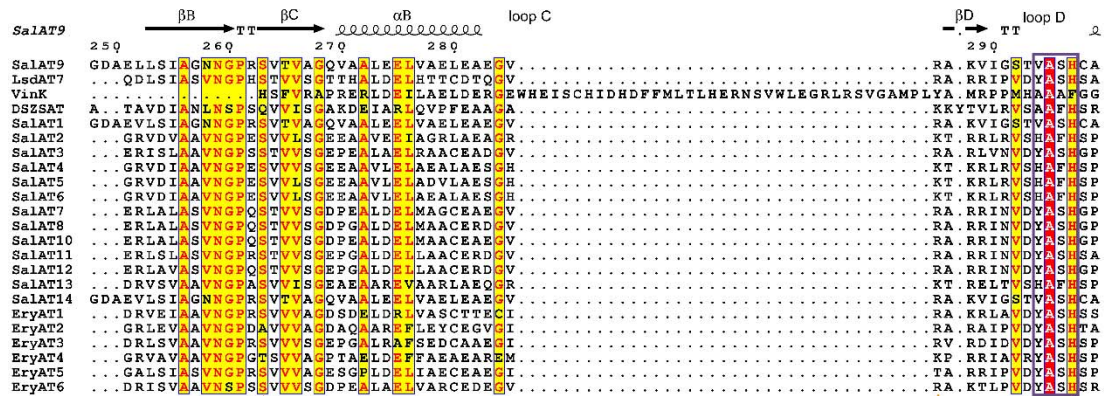
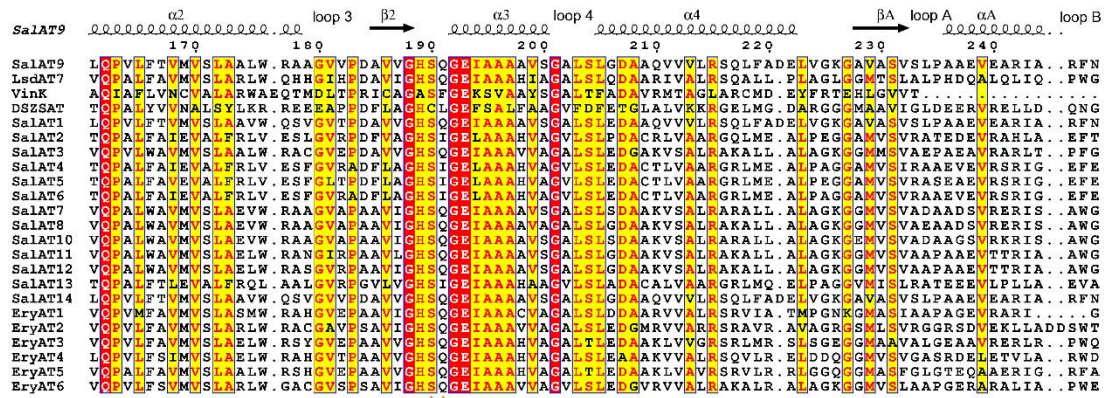
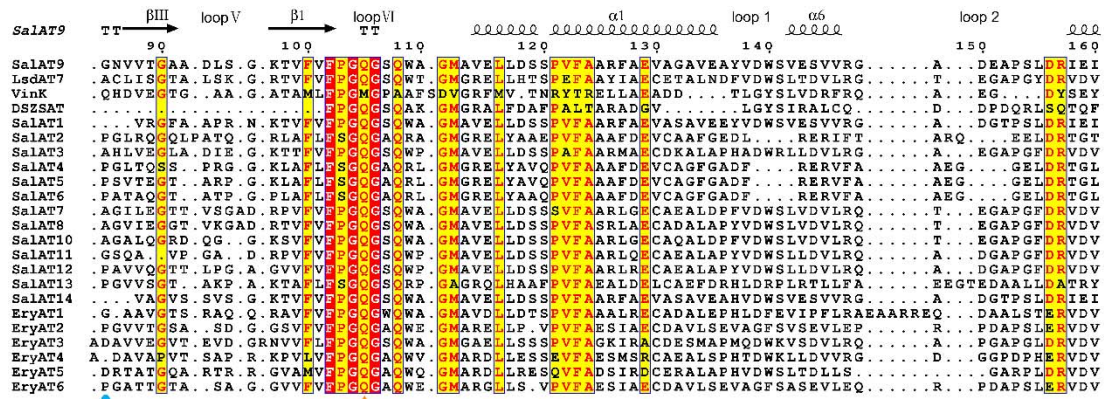
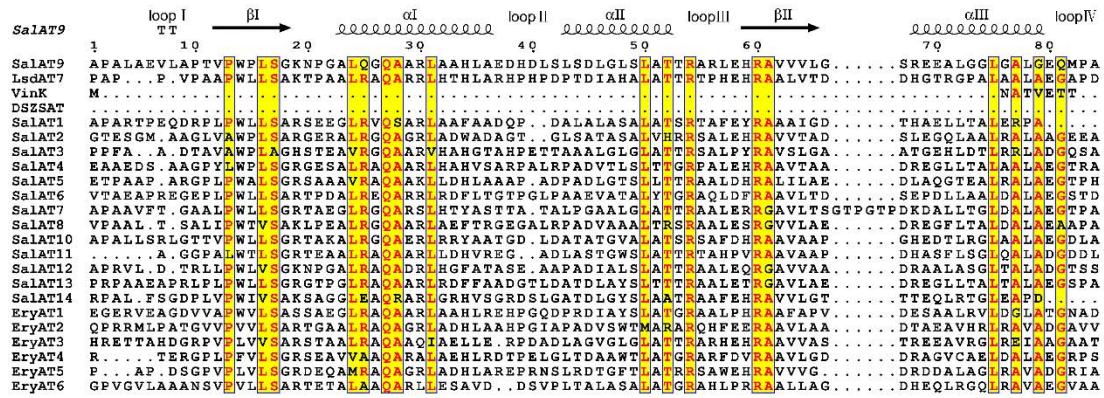


Figure S4 Cross-linking of SalAT9 and SalACP9. Undesired cross-linking is caused by the presence of C298 and C347 on the surface of SalAT9. Replacing the two cysteine residues to serine abolished the undesired cross-linking reactions.



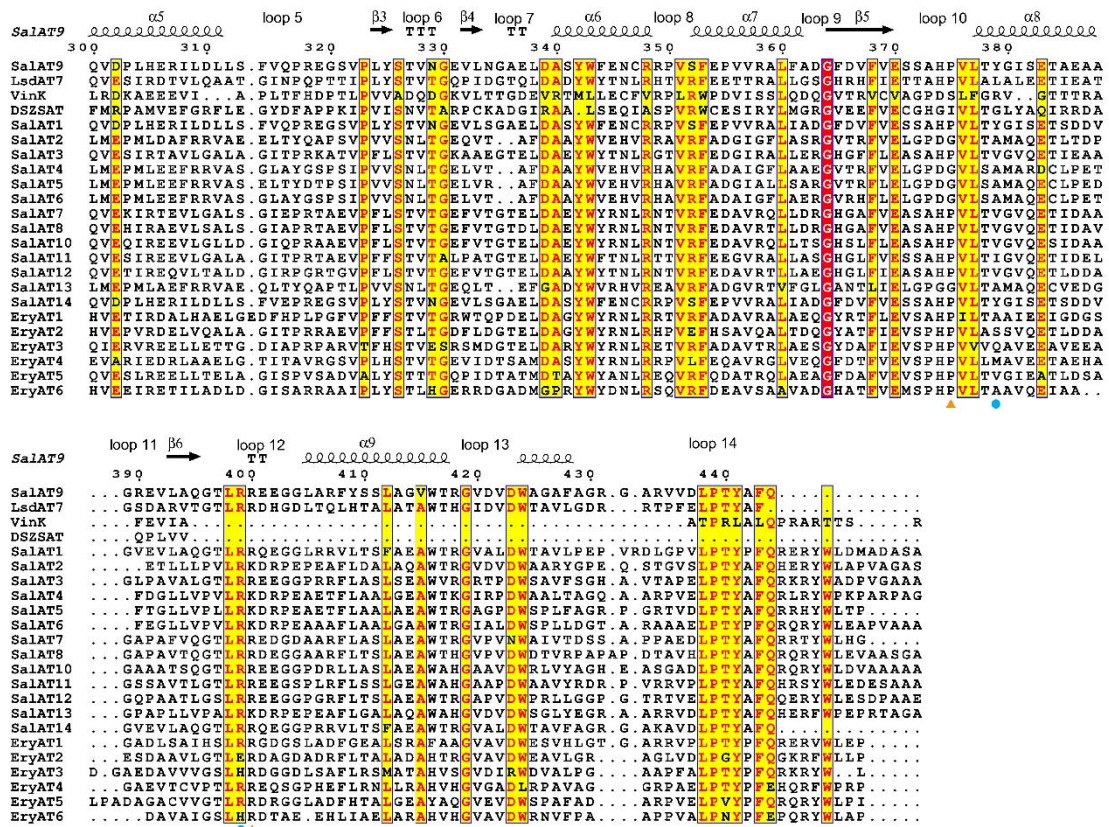


Figure S5 Sequence alignment of AT domains in salinomycin mPKS, erythromycin mPKS, Vink and DSZS AT. The secondary structural elements are indicated above the sequence. The active site of serine and histidine are indicated with red stars. The VASH motif was highlighted with purple box. The residues interacting with SalACP9 are indicated with blue circles. The residues interacting with the 4'-phosphopantetheine and BMB are indicated with orange triangles.

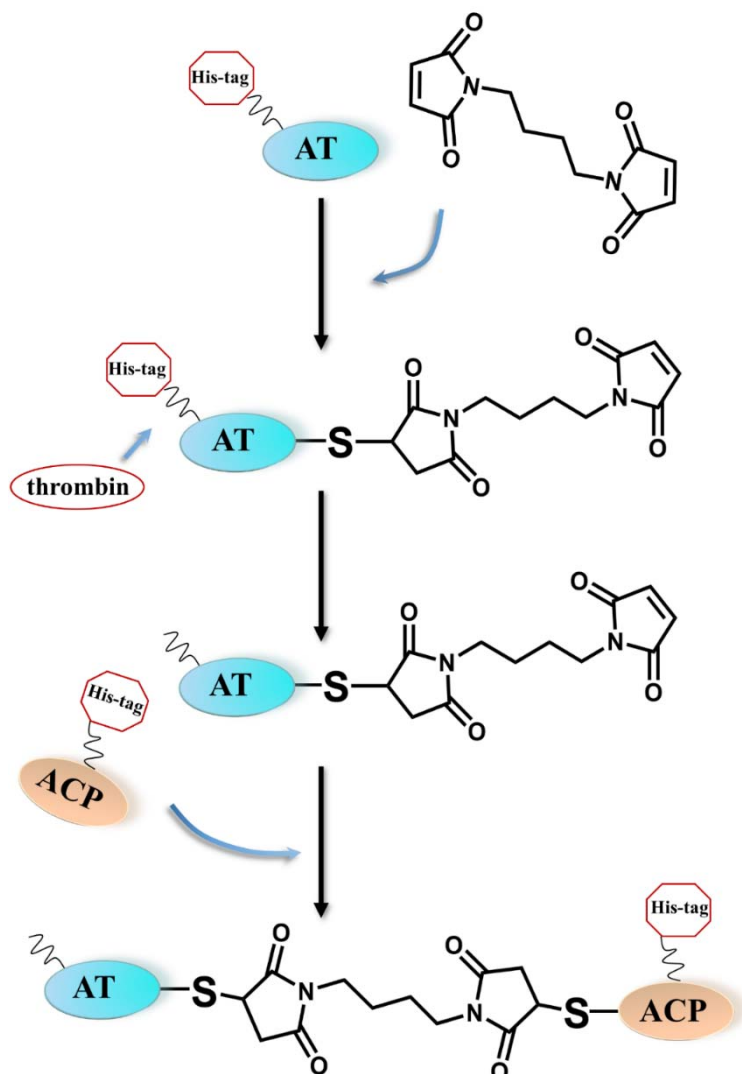


Figure S6 Crosslinking and purification of SalAT9M-ACP9 complex. The SalAT9M was incubated with BMB first, followed by removing of excessive BMB. The SalAT9M modified by BMB was incubated with thrombin to remove N-terminal His tag and then reacted with SalACP9 to obtain the covalent complex. The resulted complex was separated from the reactions by using the affinity tag of SalACP9.

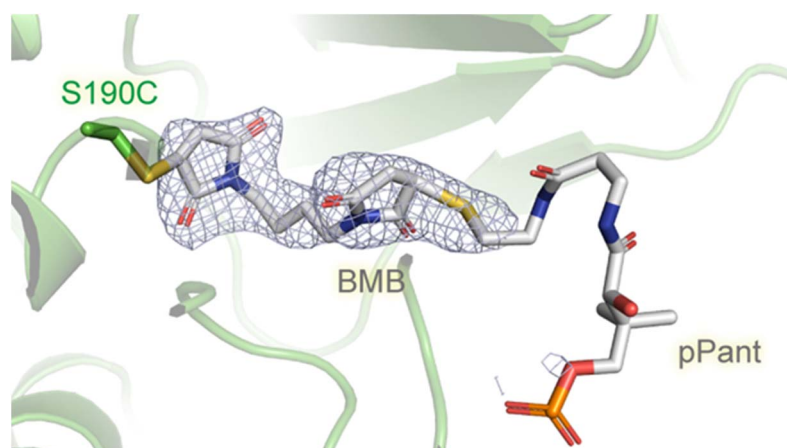


Figure S7 The electron density shows that the C190 of the standalone SalAT9M is modified by the BMB molecule. The density for the phosphopantetheine connected to BMB is barely visible. The omit Fo-Fc is contoured at 2.5σ .

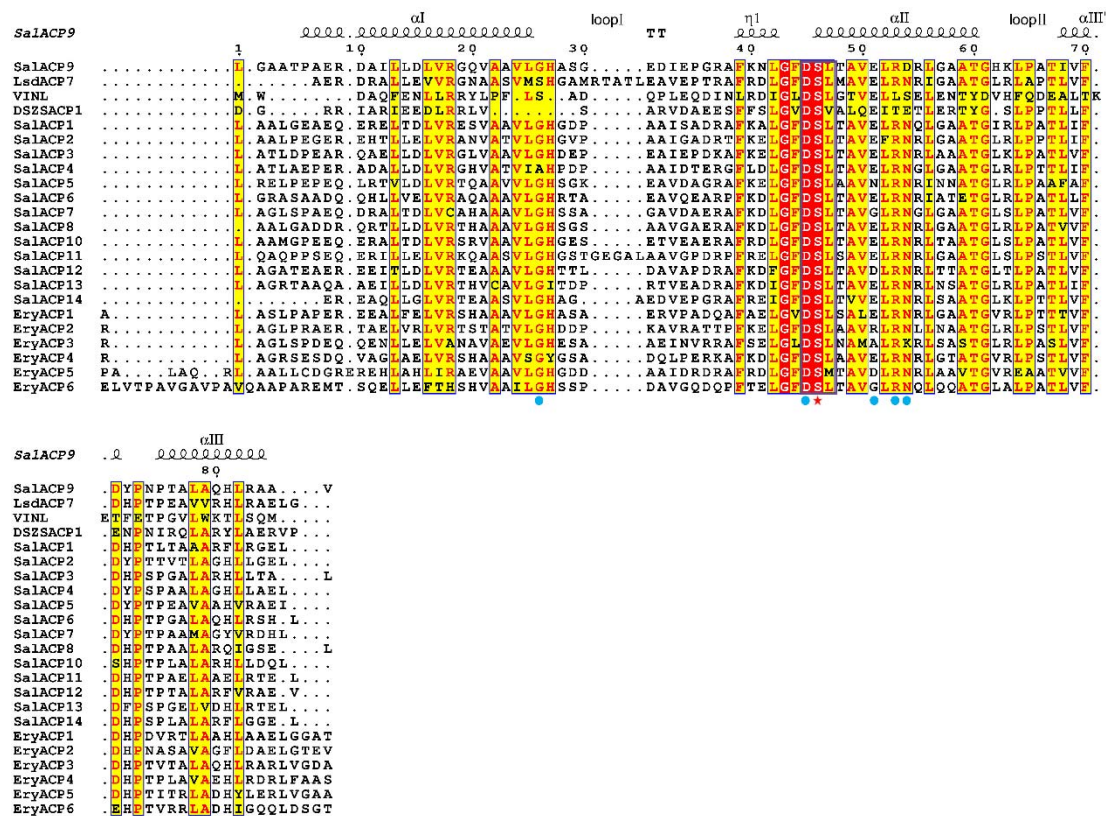


Figure S8 Sequence comparison of ACP domains in salinomycin mPKS, erythromycin mPKS, VinL and DSZS ACP1. The secondary structural elements are indicated. The active site of serine is indicated with red stars. The DSL motif was highlighted with purple box. The residues interacting with SalAT9 are indicated with blue circles.

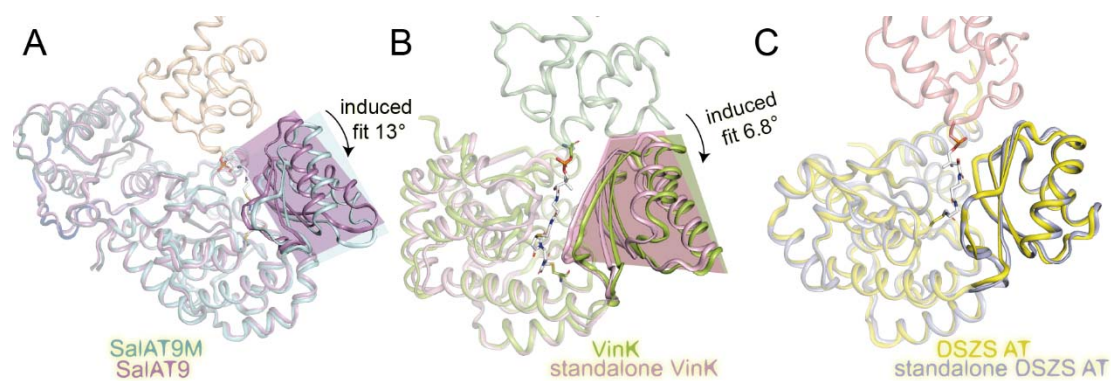


Figure S9 Conformation changes of AT small subdomain induced by ACP binding. ACP binding induces small subdomain movements in SalAT9M-SalACP9 (A), and VinK-VinL (B), but not in DSZS AT-ACP1(C)

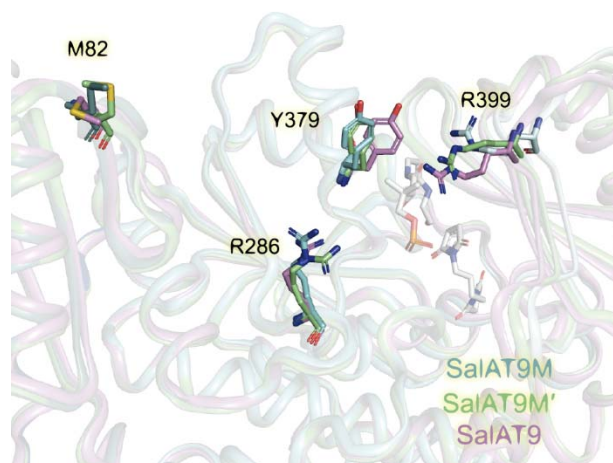


Figure S10 Conformation changes of residues induced by binding of SalACP9. SalAT9M, AT in complexes; SalAT9M', the standalone AT in the same asymmetric unit. SalAT9, AT structure crystallized in a different condition.

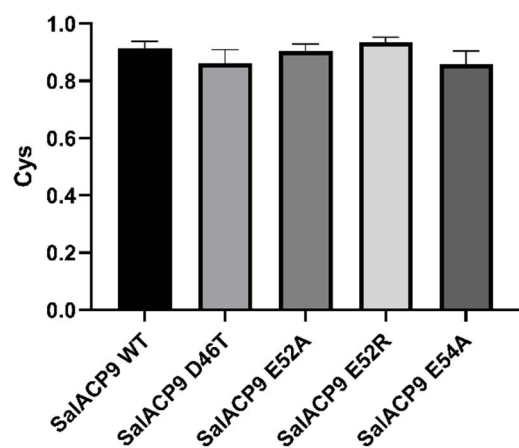


Figure S11 The phosphopantetheine sulfhydryl group of the wild-type SalACP9 and the mutants was detected by Ellman's reagent. No apparent difference in phosphopantetheinyl efficiency was observed.

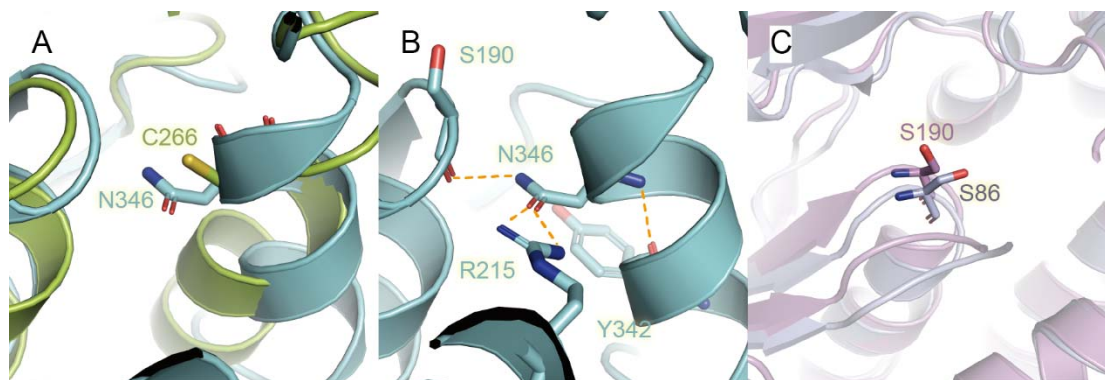


Figure S12 Comparisons of SalAT9, VinK and DSZS AT. (A) The N346 of SalAT9 corresponding to S266 of VinK, that is mutated to cysteine, is less exposed. (B) The N346 of SalAT9 forms hydrogen bonds with the side chains of R215. (C) S190 of SalAT9 correspond to the S86 of DSZS AT that was mutated to Cysteine to achieve site-specific crosslinking.

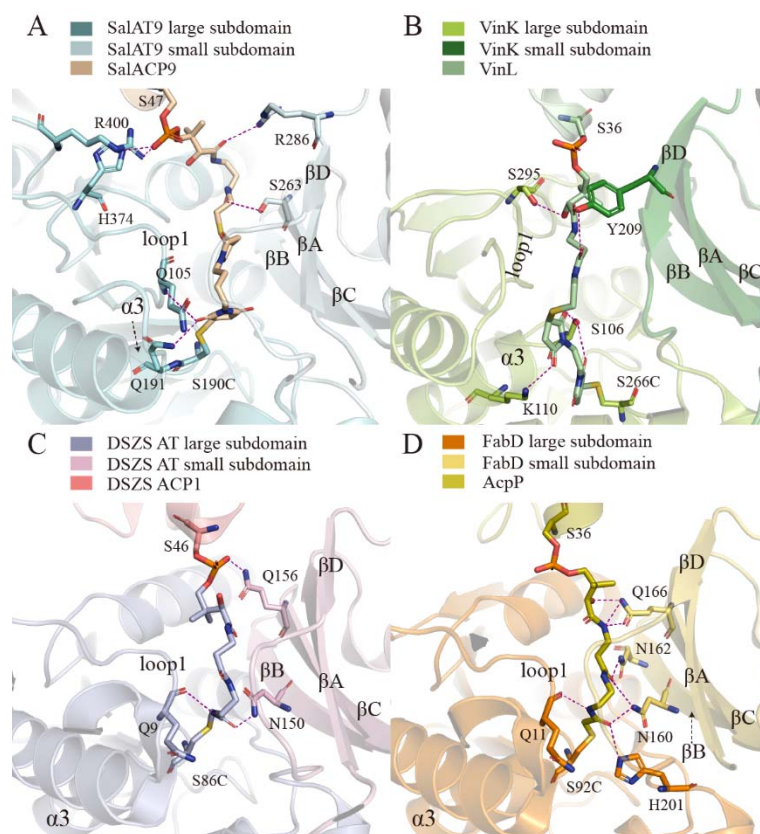


Figure S13 The position and conformation of phosphopantetheine arm in SalAT9M-ACP9(A), VinK-VinL(B), DSZS AT-ACP1(C) and FabD-AcpP(D) complexes. All phosphopantetheine arms and tunnel residues are shown as sticks. The hydrogen bonds and electrostatic interactions are indicated with purple dashed lines.

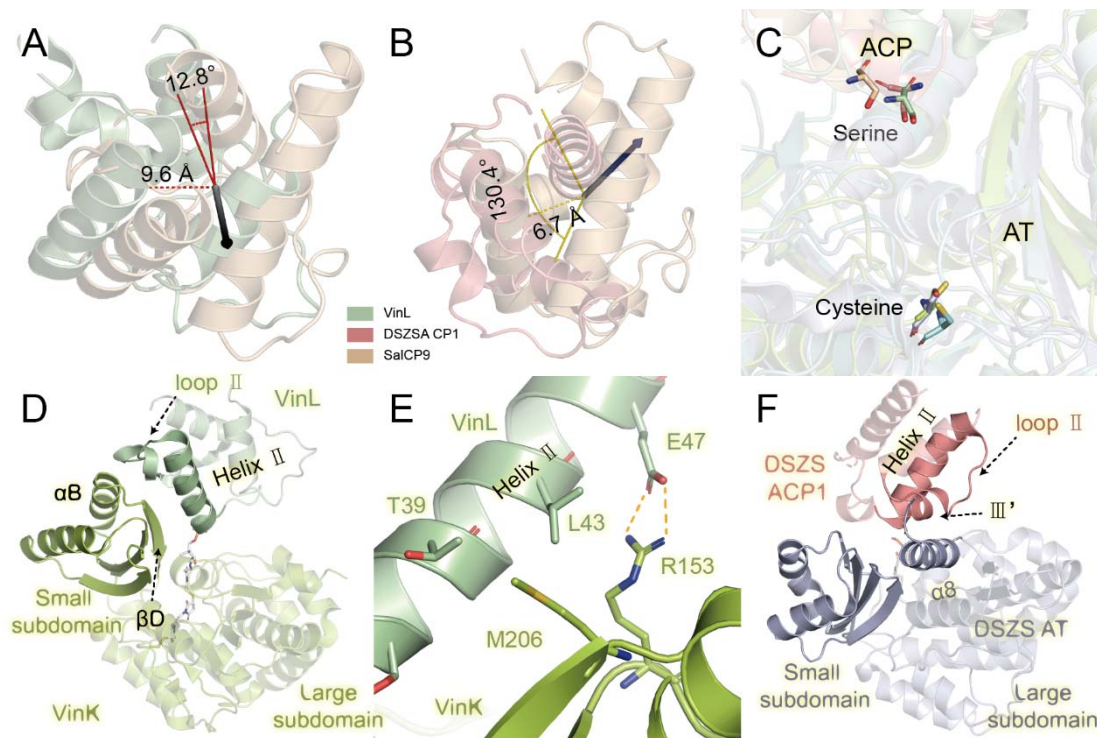


Figure S14 Structures of *trans*-AT-ACP complexes. (A) The rotation and displacement between SalACP9 and VinL are 12.8° and 9.6 Å respectively when ATs of the two complex structures are superposed onto each other. (B) The rotation and displacement between SalACP9 and DSZS ACP1 are 130.4° and 6.7 Å respectively when ATs of the two complex structures are superposed. (C) The catalytic serine residues of ACPs are positioned at the same positions in both cis- and trans-AT-ACP complexes. (D) The αII helix and the loop II of VinL pack against the βD strand and the αB helix of the small subdomain of VinK respectively in the VinK-VinL complex. (E) The αII helix of VinL contacts VinK by both salt bridge and hydrophobic interactions. (F) The short helix of the loop II (αIII') of DSZS ACP1 parallelly packs against the last helix of DSZS AT in the DSZS AT-ACP1 complex.

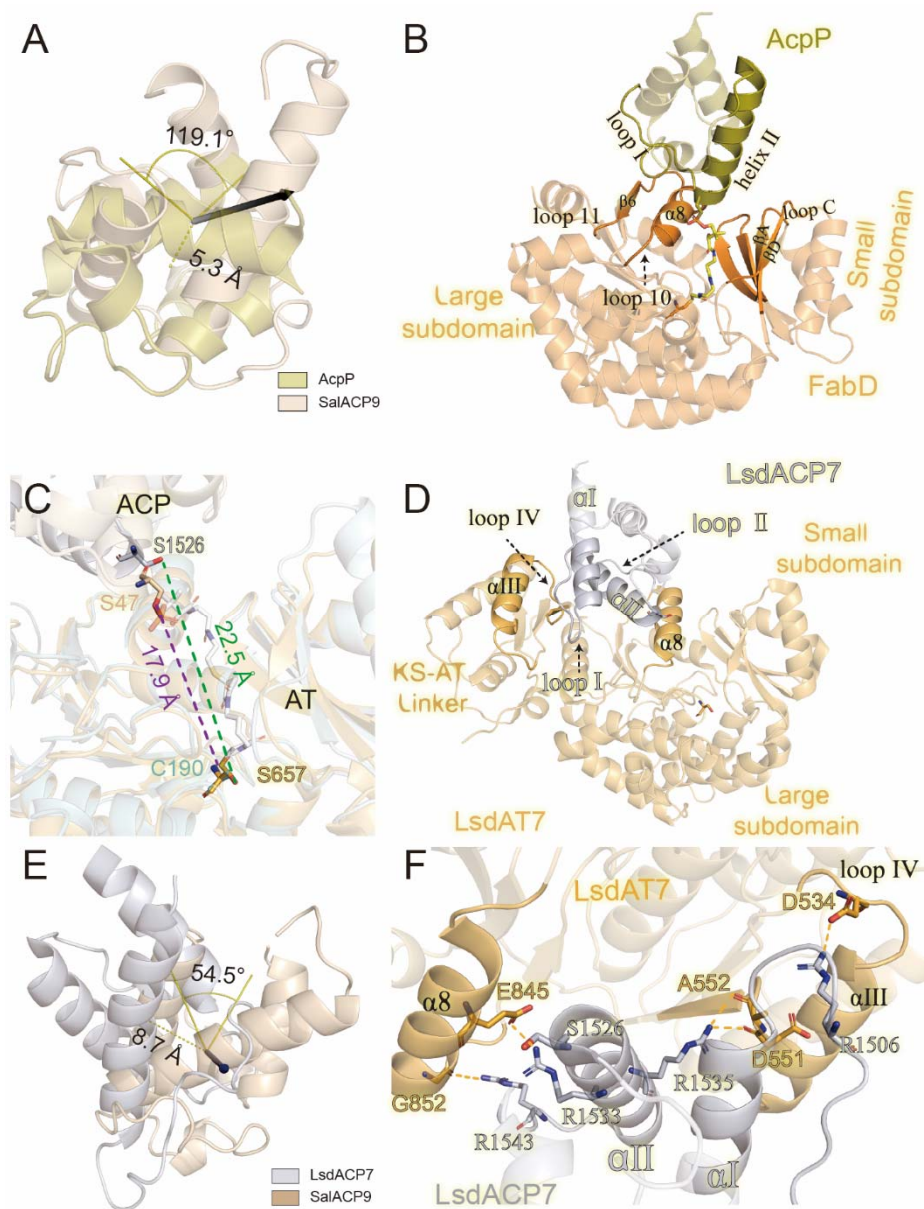


Figure S15 Structures of FabD-AcpP and Lsd14 AT-ACP complexes. (A) The orientation of AcpP in the FabD-AcpP complex structure is rotated 119.1° and displaced 5 \AA from that of SalACP9 in the SalAT-ACP9 complex. (B) FabD utilizes the $\alpha 8$, $\beta 6$ and loop10 of the large subdomain and the βA , βD and loop C of the small subdomain to interact with the helix II N-terminus and loop I of AcpP. (C) The distance between the catalytic residues S1526 of LsdACP7 and S657 of LsdAT7 is 22.5 \AA , but in the SalAT9-ACP9 complex is 17.9 \AA . (D) LsdACP7 utilizes αI , αII , loop I and loopII structural elements to make interactions with the KS-AT linker and large subdomain of LsdAT7. (E) The rotation and displacement between SalACP9 and LsdACP7 are 54.5° and 8.7 \AA respectively when ATs of the two complex structures are superposed. (F) The major interactions in Lsd14 AT-ACP complex are hydrogen bonds and salt bridge.

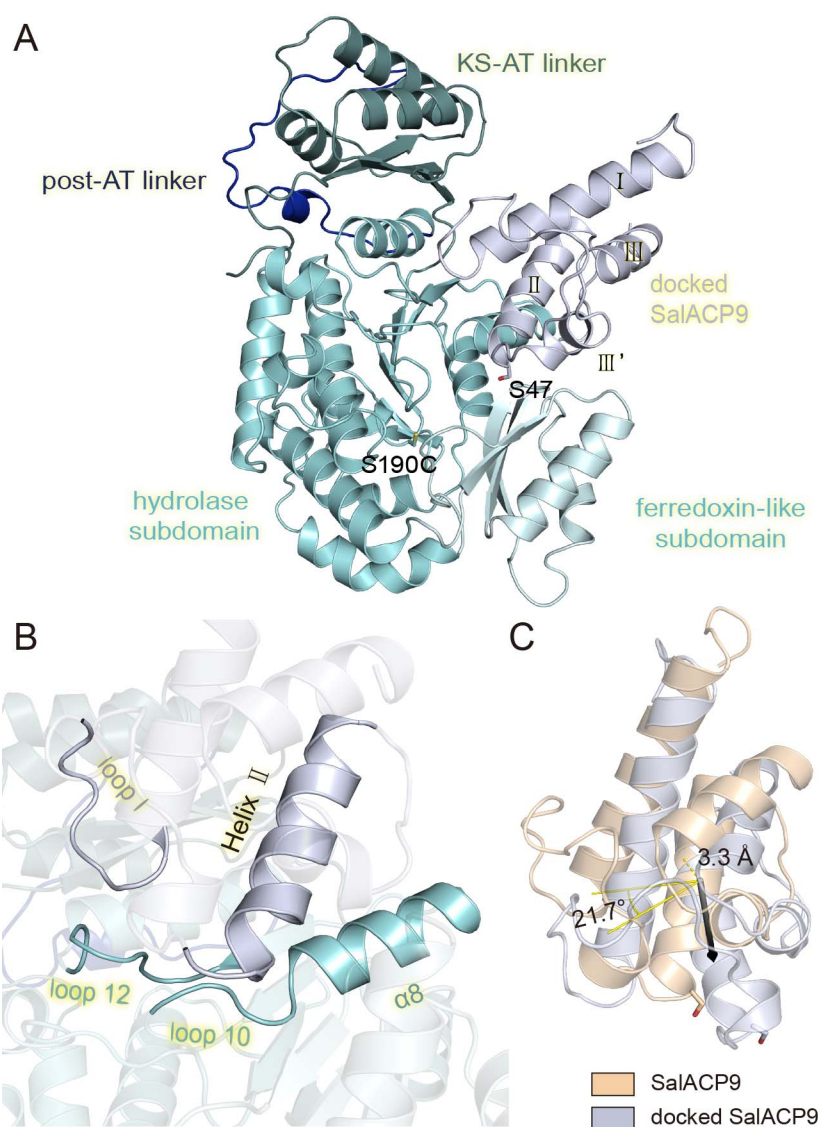


Figure S16 The docked model of SalAT9M-ACP9 by ClusPro and RosettaDock. (A) The overall structure of docked SalAT9M-ACP9. The large subdomain works as the major interaction platform, while the KS-AT linker and the small subdomain constrains the ACP binding. (B) The SalACP9 utilizes helix II and loop I structural elements to interact with the $\alpha 8$ helix, loop 10 and loop 12 of the SalAT9M large subdomain. (C) The rotation and displacement between docked SalACP9 and SalACP9 in the crystal structure of the complex are 21.7° and 3.3 Å respectively.

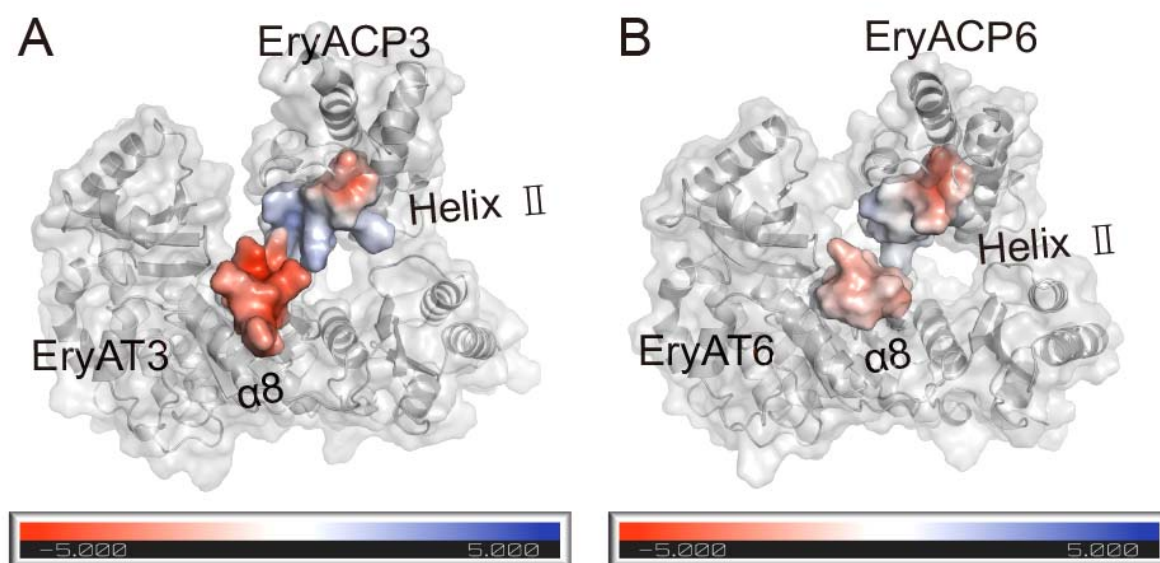


Figure S17 Electrostatic surfaces of structure elements involved in *cis*-AT-ACP interactions. (A) EryAT3-ACP3 complex. (B) EryAT6-ACP6 complex. The helix $\alpha 8$ of DEBS AT3 is more negatively charged than that of DEBS AT6, while the αII helix of the DEBS ACP3 is more positively charged than that of DEBS ACP6. Colors range from blue (positive) to white (neutral) to red (negative).